




Article

Surface and Groundwater Hydrochemistry of the Menengai Caldera Geothermal Field and Surrounding Nakuru County, Kenya

Nelly Montcoudiol ^{1,*}, Neil M. Burnside ^{1,*} , Domokos Györe ² , Nicholas Mariita ³,
Thecla Mutia ⁴ and Adrian Boyce ² 

¹ School of Engineering, University of Glasgow, Glasgow G12 8QQ, UK

² Scottish Universities Environmental Research Centre (SUERC), East Kilbride G75 0QF, UK

³ Geothermal Training and Research Institute (GeTRI), Dedan Kimathi University of Technology, Nyeri 657-10100, Kenya

⁴ Geothermal Development Company, P.O. Box 17700-20100 Nakuru, Nakuru County, Kenya

* Correspondence: Nelly.Montcoudiol@glasgow.ac.uk (N.M.); Neil.Burnside@glasgow.ac.uk (N.M.B.)

Received: 28 June 2019; Accepted: 7 August 2019; Published: 15 August 2019



Abstract: In order to assess the sustainability and impact of production from geothermal reservoirs on hydrological systems, a thorough understanding of local and regional hydrogeological systematics is a prerequisite. The Menengai Caldera in the Kenya Great Rift Valley is one of the largest explored geothermal fields in the country. This paper presents a hydrochemical investigation of the Menengai Caldera geothermal field and the ground and surface waters of the surrounding Nakuru County. Our results demonstrated a similar, sodium-alkaline dominated, ionic composition across all water types. Geothermal wells return the highest cation/anion concentrations and largely demonstrate a meteoric source from their $\delta^{18}\text{O}$ and $\delta^2\text{H}$ signature. Wells MW-09 (central part of the caldera), MW-18 (eastern part) and MW-20 (central part) showed a more evaporitic signature, closely matching with our own calculated Lake Evaporation Line, suggesting an increased mixing influence of Lake Nakuru waters. MW-09 also showed evidence of high-temperature oxygen isotopic exchange and significant water-rock interaction. Lake samples largely demonstrated seasonal shifts in ionic and isotopic values. Lake Nakuru ionic composition and isotopic values increased throughout the 12-month wet–dry–wet season sampling period. This correlated with a decrease in area which suggests a lessening of water inflow and facilitates increased evaporation. Groundwaters demonstrated clear evidence of mixing between meteoric, irrigation and lake waters. These observations enhanced the understanding of the hydrological system surrounding the Menengai Caldera and, when combined with future studies, will provide a powerful tool to assess the sustainability and impact of soon-to-be completed geothermal power production operations.

Keywords: geothermal; hydrology; hydrochemistry; water; Kenya; East Africa; Menengai Caldera; Nakuru

1. Introduction

The geothermal potential of the Kenyan Great Rift Valley (GRV) section of the East African Rift System (EARS) was first recognized in the mid-1950s [1] and is estimated to be 10,000 MWe [2]. The number of wells drilled for geothermal energy exploration and exploitation had initially been incremental, but intensity of drilling has intensified in recent years due to a rapid rise in Kenyan energy demand [3]. The latest figures show that 56% of the Kenyan population have access to electricity, but there is sizeable inequality between urban (78%) and rural (39%) areas. As of 2016, there was a diverse mix of power generation sources led by geothermal (43%), with additional inputs from hydro (34%), oil (21%), and

other renewables (biofuels, wind, solar: 2%) [4]. Following the commission of Unit 1 at the Olkaria I power plant in 1981, Kenya became the first EARS country to have significant production of electricity from geothermal energy [1], and since 2012 it has been the only producer of geothermal energy in the region [4]. Geothermal contribution to the energy mix was steady from 1990 to 2002 (c. 10%), before rapidly doubling to 19% by 2004. After a decade of slow increase, it doubled again between 2013 and 2014 to reach the most recent recorded value (Figure 1). The installed capacity for geothermal energy in Kenya is currently 727 MW after Unit I of Olkaria V came online on 27 July 2019 [5].

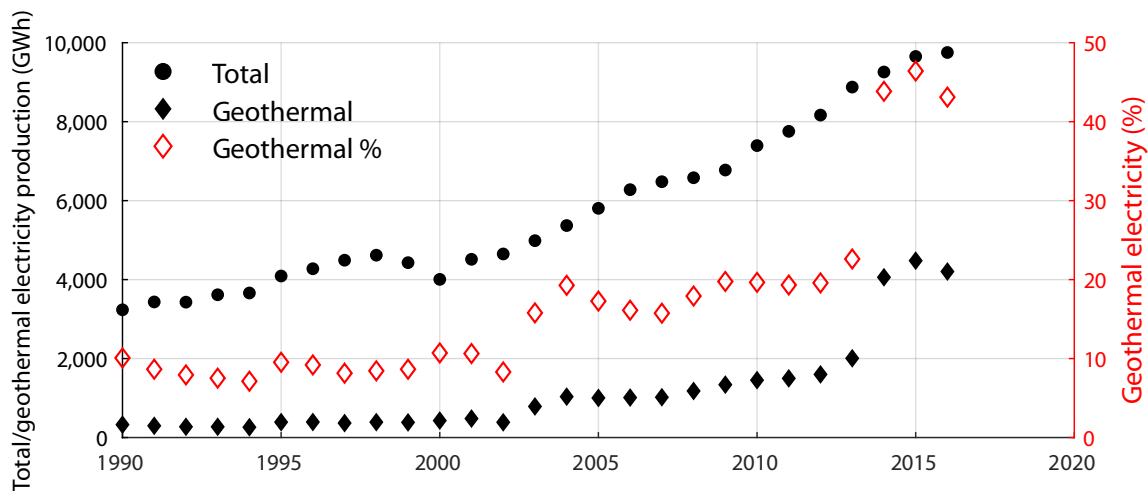


Figure 1. Evolution of electricity production and geothermal share in production for the period 1990–2015 for Kenya [4].

Exploration and development have mainly focused on high enthalpy systems as demonstrated by the >206 wells that have been drilled in Kenya into high temperature systems [6]. All of the high temperature prospects in the GRV are closely associated with Quaternary volcanoes [2]. At least 16 geothermal fields have been identified and are at various stages of exploration and development (Figure 2). This paper focuses on the Menengai geothermal field. In the following sections, we use new water chemistry and stable isotopic data to reflect on previous studies, further our understanding of the hydrogeological system which hosts the Menengai Caldera and make initial assessments of hydrological behaviour in the area.

2. Study Area

2.1. Geological Setting

The Rift Valley is made of a succession of late Tertiary and Quaternary volcanic sediments. Pre-Cambrian basement rocks are postulated to underlie this volcano-sedimentary succession at, or below, sea level [7]. The rift is defined by major Pliocene boundary faults (e.g., Mau escarpment) and a network of sub-parallel Middle and Upper Pleistocene faults that dissect the graben floor. The fault network in the rift floor is locally covered by the volcanic sediments [7,8].

The Menengai Caldera is located in the GRV, just north of the city of Nakuru and the lake of the same name (Figure 2). It represents a major Quaternary volcano located within the axis of the central segment of the GRV. The volcano is within an area characterised by complex tectonic activity associated with a triple junction fault zone [9,10] and the confluence of two major (Molo and Solai) tectono-volcanic axes (TVAs) [10–12]. The volcano is mainly composed of strongly peralkaline, silica oversaturated trachytes and has had a complex geochemical evolution, resulting from the interplay of magma mixing, crystal fractionation and liquid state differentiation [13,14]. The formation of the shield volcano began about 200,000 years ago and was followed by the eruption of two voluminous ash-flow tuffs, each preceded by major pumice falls [11–13]. More than 70 post-caldera lava flows

cover the caldera floor, the youngest of which may be only a few hundred years old [11–13]. Post caldera activity (<0.1 Ma) mainly centred on the caldera floor with eruption of thick piles of trachyte lavas from various centres [11,12].

2.2. Hydrology and Hydrogeology of the Region

Lake Nakuru is located at an elevation of 1760 m above sea level (m asl) and lies in a graben-bound internal drainage basin between the Bahati Escarpment to the east and the Mau Escarpment to the west [8,15]. Four rivers drain from the Mau Escarpment towards the lake. Most of their flow is lost to groundwater recharge before the lake is reached and only two of them (Makalia and Njoro) are normally perennial. None of the streams or rivers from the Bahati Escarpment reach the lake, and all except one (Ngosur) are seasonal in nature [8,16–18]. The Menengai Caldera (2280 m asl) is located to the north of the lake. Lake Elementaita, a high-pH soda lake rich in blue-green algae and host of hot spring activity, is situated c. 13 km to the SE and separated by a low topographic divide.

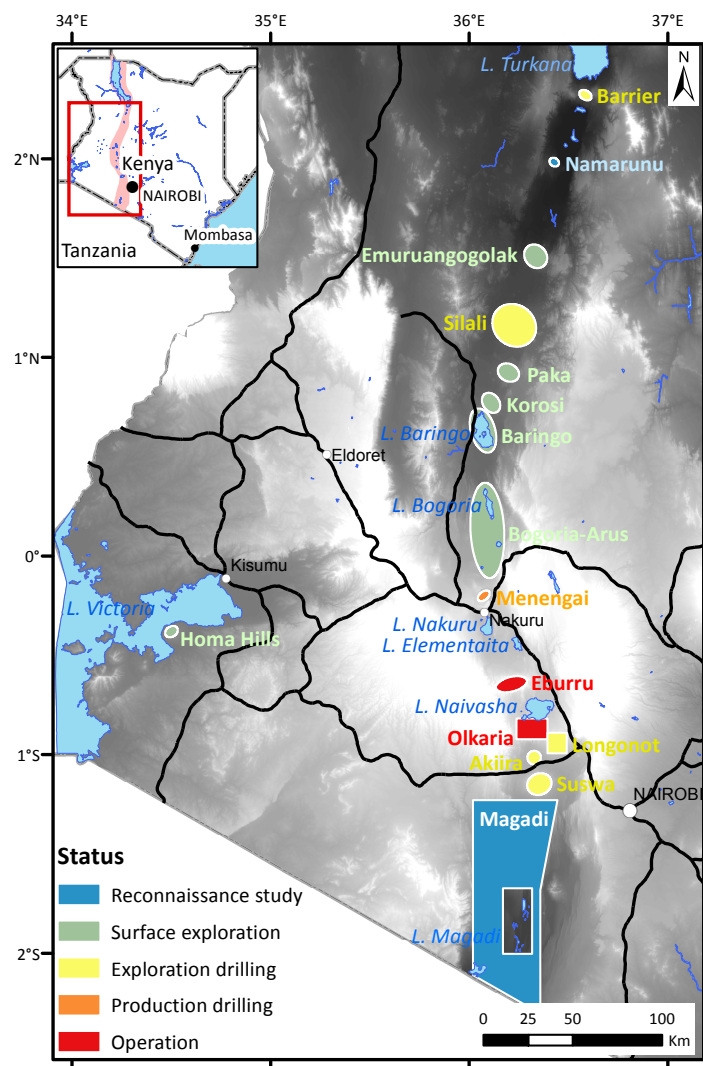


Figure 2. Map of the Kenyan Great Rift Valley showing the location of the main geothermal fields and their status as of 2018 (redrawn after [19]). The concession extent is only known for Olkaria [20], Longonot [1] and Magadi [21] fields. All the prospects (except Homa Hills) are located in an area of lower elevations (darker shades of grey) that represents the eastern branch of the East African Rift System (EARS, pink area in insert).

Hydraulic gradients suggest that shallow groundwater flows directly towards Lake Nakuru from the east and west high elevated rift edges (Mau and Bahati Escarpments), from the south (the Eburru volcano) and possibly from the Menengai Caldera. At greater depth, the regional flow is assumed to be northwards towards the low-lying area of Lake Bogoria [8]. This flow pattern is affected by the presence of the major N–S trending rift faults that act as barriers to lateral flow, resulting in deeper and longer flow paths. The fault network of the rift floor tends to align with the regional flow path that follows the rift axis. The productivity of the shallow aquifers (<200 m bgl—below ground level) is variable [8,16].

Nakuru Lake is alkaline and saline (Na-HCO₃ water type) as a result of evaporation and is recharged by rainfall, surface runoff and groundwater [8,16,18]. Treated wastewater from Nakuru also drains into the lake [16]. Groundwater around Lake Nakuru is mostly of Na-HCO₃ water type with high silica content (oversaturated in SiO₂) resulting from recharge and limited water–rock interaction [8]. The geology of the region is also responsible for high fluoride concentrations in the waters (>1.5 mg/L, guideline from the World Health Organisation—WHO) [22]. Generally there is no evidence of mixing with other water types, except for one well located NW of Lake Nakuru which demonstrates high chloride concentration and suggests some lake outflow, albeit limited or rapidly diluted by recharge from the west escarpment according to O and H isotopic data [8].

2.3. Source of Subsurface Heat in the Region

Although geological survey work regarding the region's geothermal resources in the area dates back several decades, detailed geochemical studies focusing on heat and fluid sources only started in the early 1990s [23,24]. Sources of geothermal (i.e., deep) heat have been historically constrained by the isotopic composition of volatiles with similar origin [25]. Generally, CO₂ is the most abundant component in near-surface geothermal manifestations along the Kenyan Rift (e.g., fumaroles, well gases), its isotopic composition ($\delta^{13}\text{C}$) averages c. -3.7‰ with very little variation along the ridge from Lake Magadi (to the south) to Lake Turkana (to the north) [23]. Although such a value provides no resolution between magma and carbonate derived sources [26], the regional lack of large quantities of carbonates suggests that the CO₂, and the associated heat, is magmatic in origin. The majority of recorded CO₂/³He ratios of gases ($1\text{--}10 \times 10^9$) support this hypothesis, with occasionally higher values ($10^{11}\text{--}10^{12}$) suggesting the presence of minor non-magmatic CO₂ in shallow fumaroles (e.g., Olkaria, Ol Kokwe Island) [23]. On the basis of He-CO₂ isotopic ratios in basalts [23,24], the source for mantle volatiles has been proposed to be upper mantle, identical to that of midge ocean ridge basalts (MORB), linked to Tertiary and Quaternary volcanism by [23,27], rather than lower, plume like sources identified northeast along the rift in Ethiopia [24]. In contrast, more recent studies proposed a slightly different theory which would suggest an altered ocean island basalt (OIB) like plume source under the region [28]. Magmatic fluids exploit faults to ascend into shallower crustal reservoirs, where they mix to varying degrees with cooler crustal and atmospheric derived fluids.

2.4. Geothermal Exploration and Development Efforts in the Menengai Geothermal Field

Thermal, seismic and gravity data were collected in the 1960s. These studies identified the thinning of the lithosphere below the rift [29–32]. Focused reconnaissance studies for geothermal potential were carried out in the 1980s in the region [33]. The extent of these investigations is unknown as the results are not publicly available. During this period, the British Geological Survey (BGS) carried out a hydrogeological assessment of the GRV which included Lake Nakuru and its surroundings, with no specific focus on the geothermal manifestations in the Menengai Caldera and its vicinity [8].

Limited, but promising, information for the Menengai geothermal prospect led to detailed surface exploration in 2003–2004 by KenGen [33]. These studies included: Geological and hydrogeological surveys [34], geophysical surveys (magneto-telluric and transient electromagnetic resistivity, micro-seismicity and gravimetry) to locate the heat sources [10,11,34–36], heat loss surveys [11,34,35], and geochemical surveys [33,34]. Heat losses are mainly related to the presence

of fumaroles and hot ground as no hot springs are present in or near the caldera [33]. Fumaroles, surface water, groundwater and soil gas have been analysed for their composition [12,16,33,37,38]. These studies demonstrated strong indications of an economic geothermal resource—in terms of heat in place, hydrological recharge and reservoir permeability—and were the basis for the locations of subsequent exploration wells.

Exploration drilling started in 2011 by the Geothermal Development Company (GDC) [39,40]. Over 60 wells have now been drilled at depths down to 3200 m bgl to access an estimated resource potential of at least 162 MWe (based on 40 wells [41]). Reservoir temperatures of up to 400 °C have been measured at 2000 m bgl in some wells [3,6]. The mapped potential area is c. 80 km² with a total estimated resource potential of 1600 MWe [41]. New hydrogeochemical studies [16,17,42] have been carried out since data from the drilled geothermal wells became available (summarised in Table 1), as well as geophysical surveys [38,43,44]. The conceptual model of the geothermal reservoir has been updated and refined accordingly [38,45]. Information derived from the drilled wells postulates the existence of three reservoirs in the caldera [45]:

1. A shallow liquid-dominated reservoir with temperature of 150–190 °C, intersected by wells MW-01, 03, 04 and 12, but very thin or absent in the vicinity of MW-06, 09 and 13 in the caldera centre. Estimated depth of 700–1100 m bgl at the top and 1000–1400 m bgl at the base, with areal extent of c. 20 km².
2. An intermediate reservoir with estimated temperatures in the range 250–270 °C in the vicinity of wells MW-01, 04 and 12 and c. 230 °C near MW-03. Possibly hydraulically connected to reservoir 3 (below).
3. A dome-shaped deep reservoir with temperature estimated to be between 280 °C and >340 °C which is vapour-dominated in its central part (MW-06, 09, 12 and 13); a two-phase vapour-liquid zone near MW-01 and 04; and a liquid-dominated zone near MW-01 and 03 (with MW-01 at the zone boundary). In the centre of the dome, the estimated depth is 1100–1400 m bgl at the top and 2000–2200 m bgl at the base, with an average 600–1000 m thickness that decreases to below 500 m at the peripheries.

Fluid geochemistry is similar in all cases and is sodium-bicarbonate (Na-HCO₃) water type with concentrations in sodium in the range 2500–3500 mg/L and bicarbonate between 4800–8500 mg/L. Recorded non-condensable gases (NCGs) are dominated by CO₂, with proportion ranging from 10% *w/w* near MW-01 to <4% *w/w* near MW-13 and MW-09 [38]. NCGs are thought to be accumulating at the top of the deep reservoir due to boiling conditions, with the actual reservoir content being much smaller [45].

Steam production from individual wells varies but can reach in excess of 10 MWe, when combined the production from all wells equates to >100 MWe of steam equivalent [6]. Three companies have each secured a 20-year license to operate 35 MWe modular plants [3]. GDC is currently undertaking production drilling to deliver resource access for the total 105 MWe power development [2]. Quantum Power East Africa was scheduled to start construction in September 2018, after securing funding from the African Development Bank (AfDB), and the two other companies (OrPower22 and Sosian Menengai Geothermal Power) were scheduled to start shortly afterwards [46]. In April 2019, Chinese company Kaishan Renewable Energy Development signed contractual agreements with Sosian Menengai Geothermal Power for procurement, engineering and construction (EPC) and to operate and maintain the future Menengai III geothermal power plant for a period of 14 years [47].

Table 1. Summary of hydrogeochemical studies publicly available focusing on Menengai geothermal field (from oldest to most recent).

Sampling Features	Available Data	Main Findings	Reference
MW-01	Water chemistry, gas analyses, temperature and pressure profiles	Two main feed zones with potential mixing; 2-phase fluid rich in CO ₂ and oversaturated with respect to calcite CO ₂ from magnetic flux rather than equilibrium with minerals	[48]
MW-01, MW-04 and MW-05; lakes; cold and hot springs; boreholes	Water and gas chemistry, H and O isotopes	Menengai geothermal fluid is a mixture of local groundwater and water from Lake Nakuru Isotopic signature affected by water-rock interaction in MW-05	[42]
MW-01 and MW-04; Lake Nakuru; boreholes	Water chemistry, H and O isotopes	Geothermal reservoir fluid, Lake Nakuru waters and local groundwater align on a possible mixing line Other hypothesis suggested: Rock-water interactions or dilution by local meteoric water Possible mixing between two end-members (feed zones)	[16]
MW-01, MW-03, MW-04 and MW-12 (two-phase discharge); MW-06 and MW-09 (steam)	Water chemistry, non-condensable gases	Steam fraction 0.1–0.5 Silica used as geothermometer Fluid gas concentrations increasing with temperature Dissolved CO ₂ controlled by local equilibrium between fluid and secondary minerals; some input due to magmatic intrusion	[49]
MW-01, MW-03, MW-04, MW-12, MW-19 and MW-20	Water chemistry, gas composition	Heterogeneous reservoir with excess enthalpy caused by phase separation and conductive heat transfer from hot rock or magma to the circulating fluid, forming superheated steam	[50]
MW-01, MW-03, MW-04, MW-12, MW-19 and MW-20 (two-phase discharge); MW-06, MW-09 and MW-13 (steam)	Gas composition	Low H ₂ O/CO ₂ related to high temperature from deep horizons and conversely Wells producing steam richer in H ₂ S than 2-phase wells Redox conditions controlled by Fayalite–Hematite–Quartz buffer Variable steam fraction; gases attain chemical equilibrium	[51]
Boreholes	Water chemistry	No impact of geothermal exploitation on groundwater resources Trend following the direction of the Molo TVA	[52]
Fumaroles	Gas composition	Temporal variations difficult to assess due to atmospheric contamination (natural or due to sampling). Nevertheless, it was concluded that no significant changes occurred in response to geothermal exploitation	[53]
MW-01A	Water chemistry	Scaling potential assessed by chemical modelling Risks of calcite scaling during initial boiling, not at later stages; of amorphous silica scaling during use of water especially if the temperature drops below 100 °C	[54]
MW-01 and MW-04; lakes; boreholes	Water chemistry, H and O isotopes, tritium	Geothermal reservoir fluid, Lake Nakuru waters and local groundwater align on a possible mixing line (same as [16]) Low tritium values suggesting mean residence time over 25 years Recharge to geothermal reservoir from Lake Nakuru (estimated at 20%)	[17]
Boreholes; MW-01, MW-01A, MW-03, MW-04, MW-09A, MW-12, MW-19, MW-19A and MW-20A	Water chemistry (pCO ₂), isotopes ($\delta^{13}\text{C-CO}_2$, $^3\text{He}/^4\text{He}$)	pCO ₂ used to map structures Presence of CO ₂ in significant proportions affects boiling and phase conditions in wells Main CO ₂ origin from mantle (+ possible contribution from thermogenic processes and calcite dissolution)	[55]
Fumarole MF-2; MW-18A	Gas composition, water chemistry	Fumarole MF-2 indicates a potential permeable zone (upflow zone) Liquid chemistry of MW-18A suggests intense boiling and water–rock interaction; oversaturation with respect to calcite; minimal mixing Low gas concentrations in MW-18A vapour phase (NCG 1.6% w/w); CO ₂ dominant	[56]

3. Materials and Methods

The data collected for this study incorporates three separate field trips which took place between: (1) 27 June and 5 July 2016; (2) 14 and 22 January 2017; and (3) 1 and 12 June 2017. Samples included geothermal wells, groundwater boreholes, lakes, rivers and meteoric waters (Figure 3). A full table of field data and laboratory results are available in Tables S1 and S2. All geothermal reservoir waters were sampled at the weir outflows, situated post-fluid flash and steam release, of active production test wells (Figure 4).

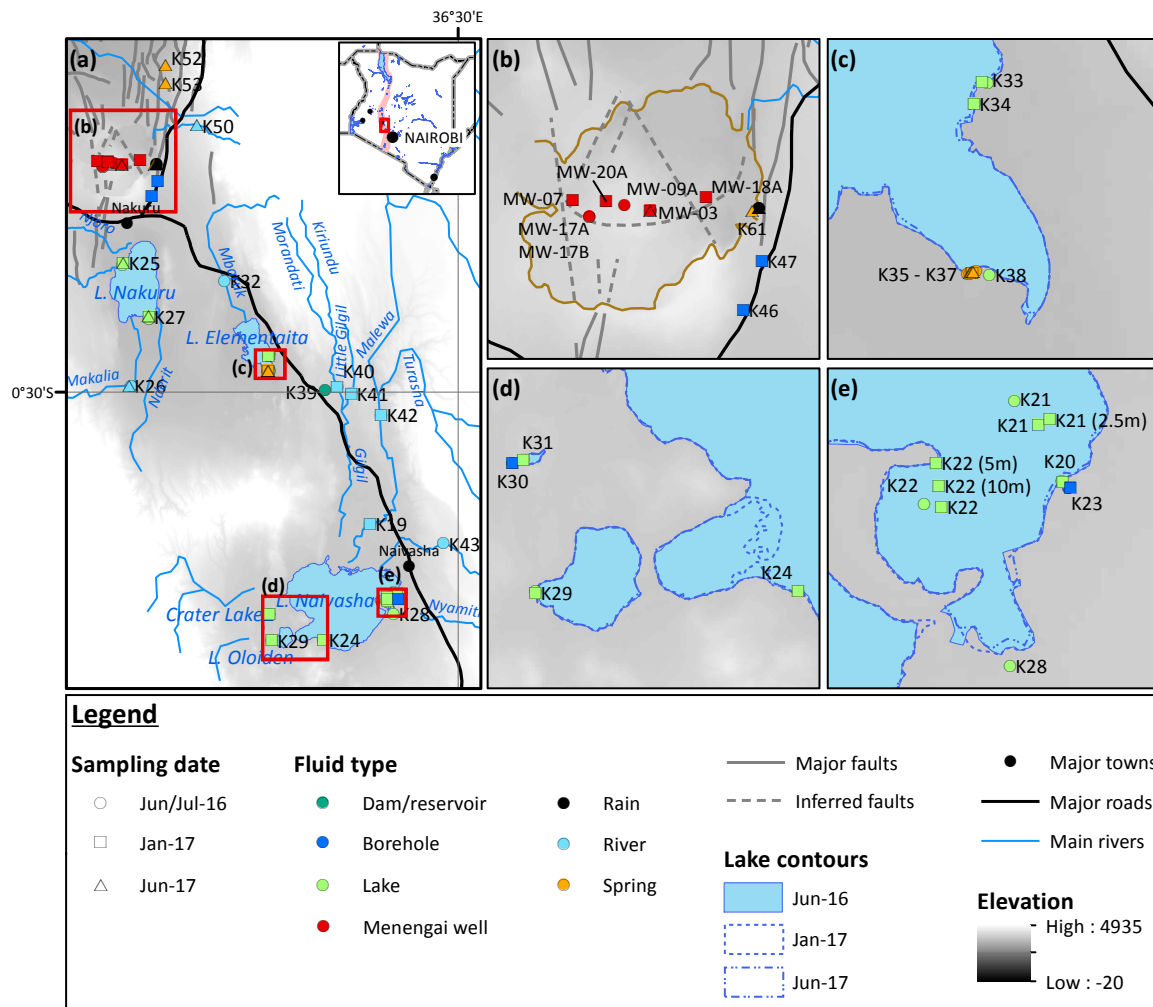


Figure 3. Locations of sampling points. (a) Entire study area; (b) Menengai Caldera; (c) Southeast shore of Lake Elementaita; (d) Southwest shore of Lake Naivasha, Lake Oloiden and Crater Lake; (e) East shore of Lake Naivasha. The faults were compiled from the available literature [17,33–35,42,44,54,56]. Lake shoreline indicators were digitised from Sentinel-2 and Landsat-1 satellite imagery [57] at the relevant dates.

3.1. Field Sampling

Prior to sampling, physiochemical water parameters were measured in the field: Temperature, electrical conductivity (EC), pH and oxidation-reduction potential (ORP) were measured with a handheld Myron P Ultrameter II 6PFC instrument (Myron L., Carlsbad, CA, USA). Alkalinity was determined as CaCO₃ with a Hach Model 16,900 digital titrator (Hach, Manchester, UK), using sulphuric acid (0.16 or 1.6 M depending on measured conductivity) and pH indicators (bromocresol green—methyl red and phenolphthalein depending on pH value). Where required, equipment was

calibrated before each day's fieldwork. All water samples were refrigerated as soon as possible after collection, but in some cases were occasionally subject to periods of time when refrigeration was not possible, either in accommodation or during transit back to the UK.

Major ion samples were taken in duplicate using polypropylene screw-cap vials and filtered at 0.2 μm to remove particulate matter. Field samples of water for $\delta^{18}\text{O}$ and $\delta^2\text{H}$ were taken in triplicate using clean 10 mL glass vials with screw caps. To ensure a tight seal and prevent any evaporation of samples, caps were sealed with Parafilm.



Figure 4. Menengai production test well infrastructure. (a) MW-17a (UTM 0171344, 9976440) flashing silencer and steam release chambers showing the weir sampling location. (b) Close-up of MW-17a silencer entry demonstrating significant silica precipitation. (c) Weir outlet and sampling location for MW-09 (UTM 0172910, 9976964). All images taken by N.M.B.

3.2. Laboratory Analyses

Anion and cation concentrations were determined simultaneously using ion chromatography on Dionex equipment in the School of Engineering lab at the University of Glasgow, as described in [58]. Analysis included a 3-level calibration using ThermoFisher Combined Six Cation Standard-II and Combined Seven Anion Standard I (ThermoFisher, Loughborough, UK). Further quality control checks were completed by converting lab and field alkalinity results to meq/L (milliequivalent) and performing cation–anion balance (CAB) calculations. Of the 67 unique samples analysed, nineteen had a CAB within $\pm 5\%$ (typically regarded as accurate for all uses [59]), sixteen between 5–10%, and a further thirteen between 10–15% ($\pm 15\%$ is typically regarded as serviceable for cautious interpretation [60]). Seven samples returned a CAB of 15–20% and the remaining twelve samples were largely in the 20–25% range, and so represent values of lesser confidence for use in interpretation. Given the positive analytical checks, we believe sample preservation and alkalinity titration, which were performed and interpreted by different operators, were the main cause of the comparatively large balances.

Water stable isotope analyses were undertaken at the SUERC laboratories in East Kilbride, UK following the procedure described in [58]. Final values for $\delta^{18}\text{O}$ and $\delta^2\text{H}$ are reported as per mil (‰) variations from the V-SMOW standard [61] in standard delta notation. Repeated analyses of water standards (international standards V-SMOW and GISP, and in-house standard Lt Std) gave a reproducibility better than $\pm 0.3\text{‰}$ for $\delta^{18}\text{O}$ and $\pm 3\text{‰}$ for $\delta^2\text{H}$.

4. Results

4.1. Physico-Chemistry of Nakuru County Waters

Results from field measurements and lab analyses are summarised in Tables 2 and 3, respectively. All the results are available in Tables S1 and S2.

4.1.1. Geothermal Fluids

Hot geothermal fluids from Menengai wells are characterised by high dissolved mineral content ($\text{EC} > 3000 \mu\text{S}/\text{cm}$) and alkaline pH (> 8.8). Redox conditions are largely reducing in the Menengai wells and alkalinity values are high ($> 3700 \text{ mg}/\text{L CaCO}_3$; Table 2). Given the post-steam release sampling location, the chemistry may not directly reflect that of the reservoir. Precipitation of silica on pipe infrastructure was prevalent at each well location (Figure 4). Though this material was not sampled, co-precipitation of additional species have been previously demonstrated (e.g., NaCl [62], CaSO_4 [50]), so it is possible that some ionic components have been lost by precipitation prior to sampling activities. Despite this consideration, the range of ionic values resulting from our analyses (Table 3), were in close agreement with ranges described in previous works (see references in Table 1), with the relatively wide range of values reflecting the variability observed across different wells within the Menengai Caldera. Sodium (Na^+) and bicarbonates (HCO_3^- or CO_3^{2-} carbonates—depending on the pH) are the dominant cation and anion respectively (Na-alk water type; Figure 5). Due to the production testing schedule of geothermal well, MW-03 was the only well sampled during each separate field visit (three times in total). Ions in high concentrations (Na^+ , SO_4^{2-} , Cl^- , F^-) showed close consistency across all three field samples (Figure 6a). Ammonium (NH_4^+), nitrite (NO_2^-) and phosphate (PO_4^{3-}) were consistently below detection limit for all geothermal well samples.

Table 2. Summary of measured field determinations along the studied section of the Kenyan Great Rift Valley.

Sample Origin	Number of Samples	Temp °C	EC ¹ µS/cm	pH	ORP ² mV	Alkalinity mg/L CaCO ₃
Menengai wells	9	>65	7645–18,150	8.8–10	<–100	3780–7860
Kikopey hot springs	9	36–46	3170–4427	8.9–9.3	21–104	560–1500
Other springs	3	25–27	244–434	7.3–8.1	115–135	94–128
Boreholes	6	18–38	747–2202	7.1–8.9	107–198	235–920
Rivers	15	15–26	69–389	6.2–8.6	33–259	17–228
Lake Nakuru	6	19–33	8160–9713	9.4–9.8	17–131	340–4830
Lake Elementaita	5	23–26	11,900–13,250	9.4–9.9	1.1–164	3140–3830
Lake Naivasha	14	21–31	245–752	6.8–8.7	102–223	65–130
Lake Oloiden	2	24–30	2492–2693	9.2–9.5	129–161	960–1110
Crater Lake	2	23–25	7530–8221	9.5–9.8	86–107	3340–3380

¹ Electrical conductivity, ² Oxidation-reduction potential.

Table 3. Summary of major cation and anion lab analyses. All results in mg/L.

Sample Origin	Ca ²⁺	Mg ²⁺	Na ⁺	K ⁺	NH ₄ ⁺	Cl	SO ₄ ²⁻	NO ₃ ⁻	NO ₂ ⁻	PO ₄ ³⁻	F ⁻	Br ⁻	Li ⁺
Menengai wells	4.3–761	0.9–248	1923–5774	198–1212	n.d. ¹	425–1415	72–392	n.d.–1.4	n.d.	n.d.	77–691	n.d.–39	1.2–19
Kikopey hot springs	4.7–15	0.1–17	736–1160	26–162	n.d.	294–632	57–267	n.d.–1.9	n.d.	n.d.	86–501	n.d.–21	57–262
Other springs	0.8–3.5	9.9–14	42–98	0.2–0.4	8.9–22	5.4–15	6.7–7.7	4.5–35	n.d.	n.d.	0.7–4.5	n.d.–0.1	n.d.
Boreholes	2.7–65	1.7–16	166–499	0.9–51	n.d.	7.2–130	13–84	n.d.–26	n.d.–0.3	n.d.–1.3	5.8–9.4	n.d.–16	n.d.–7.4
Rivers	3.6–22	0.8–5.2	6.8–41	3.6–37	n.d.–5.6	0.5–31	2.1–17	n.d.–6	n.d.–0.2	n.d.	0.2–5.3	n.d.–3.6	n.d.–0.2
Lake Nakuru	6.2–17	n.d.–11	2323–2854	119–323	n.d.	679–810	63–78	n.d.	n.d.	n.d.	67–346	n.d.–6.2	n.d.–3.2
Lake Elementaita	10–53	n.d.–25	3223–3704	201–457	n.d.–63.2	1857–1986	131–166	n.d.	n.d.	n.d.	288–1298	5.3–27	0.3–9.7
Lake Naivasha	11–23	4.4–4.9	22–26	14–21	n.d.–2.1	8.1–14	0.5–3.3	n.d.–0.1	n.d.	n.d.	0.9–1.2	0.1–0.4	n.d.–0.2
Lake Oloiden	12–15	6.2–11	594–629	117–144	n.d.	85–102	1.3–2.1	n.d.	n.d.	n.d.	19–84	2.6–3.1	0.5–1.6
Crater Lake	13–28	10–16	2005–2338	340–408	n.d.	218–264	52–58	n.d.	n.d.	n.d.	78–311	4.3–5.8	0.5–3.4

¹ n.d. = not detected (below analytical technique measurement limits).

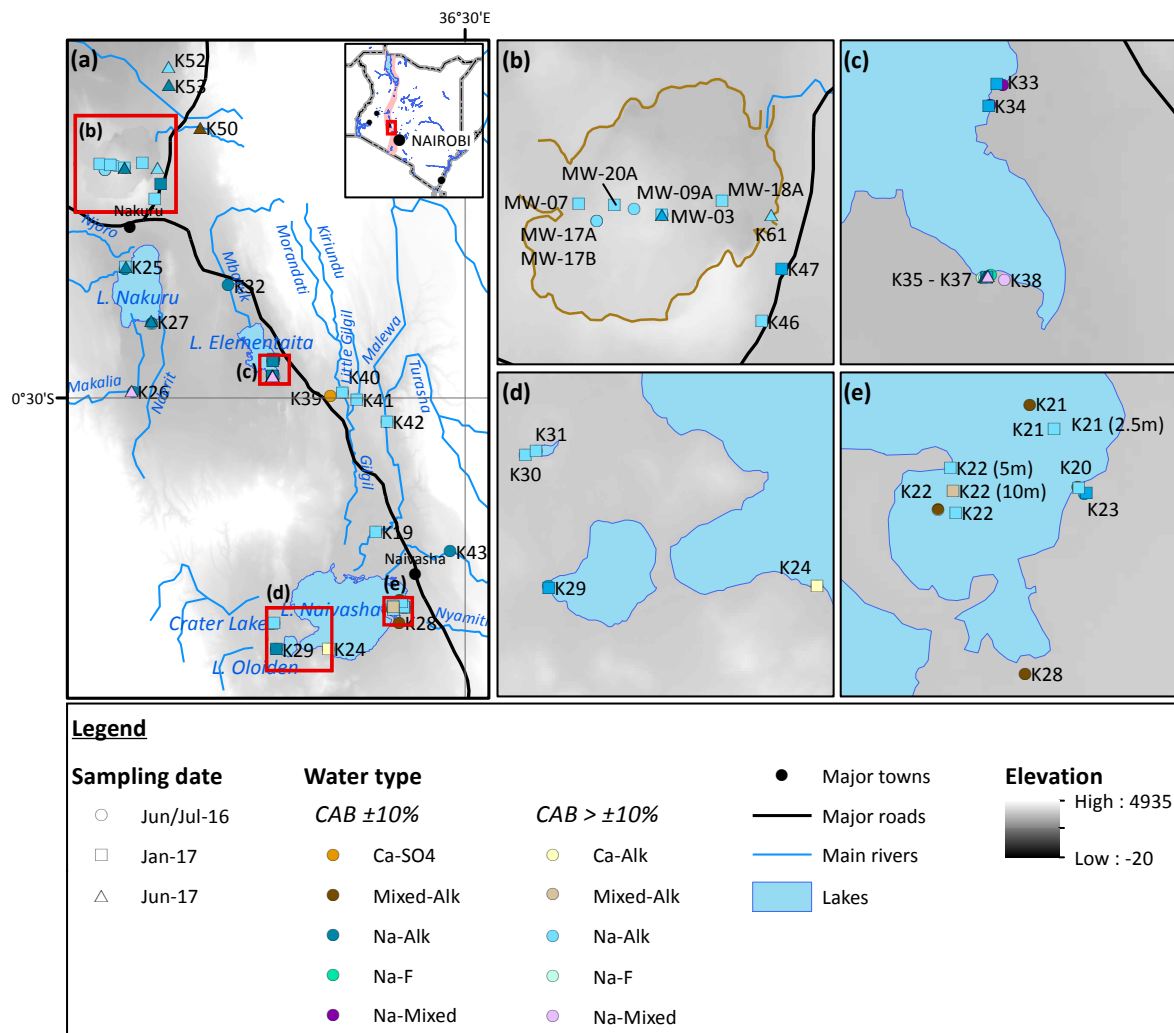


Figure 5. Fluid water type. (a) Entire study area; (b) Menengai Caldera; (c) southeast shore of Lake Elementaita; (d) southwest shore of Lake Naivasha, Lake Oloiden and Crater Lake; (e) east shore of Lake Naivasha. CAB: cation-anion balance.

The Kikopey hot spring outflows on the shore of Lake Elementaita showed high values and little variability EC and pH (Table 2). All but one well sample was within a CAB of ±15% (Table S2). Cation and anion concentrations showed some temporal variation (Table 3). The pools sampled in July 2016 were rich in fluoride compared to subsequent sampling (3–5 times higher; Table S2; Figure 6b). Sodium was the dominant cation whereas there was no common dominant anion (mixture of HCO_3^- , Cl^- and/or F^- ; Figure 5).

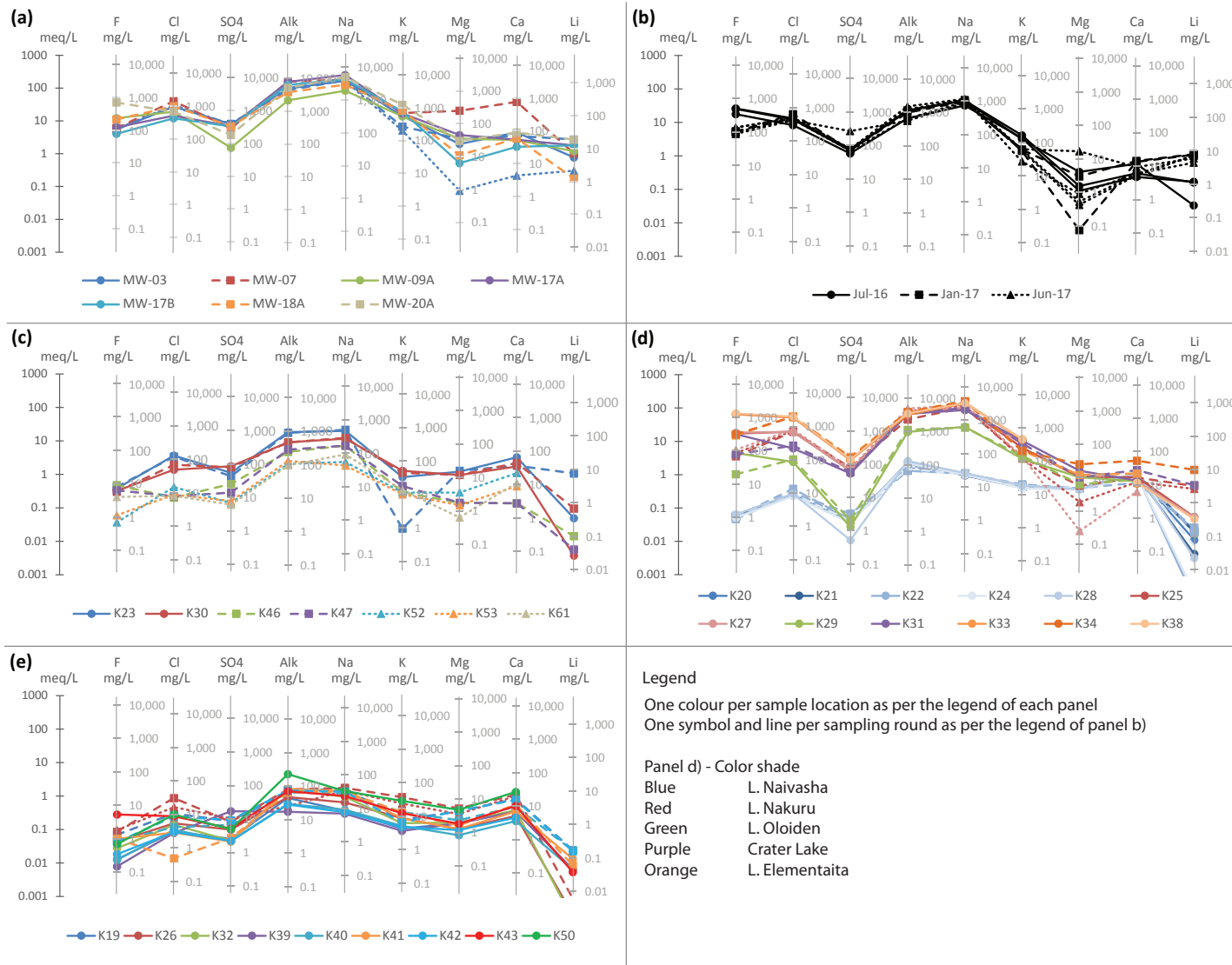


Figure 6. Schoeller diagrams. (a) Menengai wells; (b) Kikopey hot springs; (c) boreholes and cold springs; (d) lakes; (e) rivers.

4.1.2. Groundwater

Groundwater samples were collected from natural ambient temperature springs and drinking water wells. Three springs (with $T = 25\text{--}27\text{ }^{\circ}\text{C}$) were sampled in June 2017 (K52–53 and K61; Figure 3). They are characterised by low EC values, near-neutral pH and low alkalinity values (Table 2). EC, alkalinity values and ion concentrations were significantly lower than those from groundwater wells and in the same range to the rivers suggesting limited rock-water interactions due to short residence times in the subsurface (Tables S1 and S2; Figure 6c,e). All three springs are of Na-HCO₃ water type (Figure 5; Table S2) and have nitrate (NO₃[−]) and ammonium (NH₄⁺) concentrations above the detection limit (Table S2). This may be linked to farming-related activities. Springs K52 and K53 are located in an area of intensive agriculture where the use of fertilizers is likely. K61 is located inside the caldera at the base of a cliff (east edge), which, based on the topography, is draining the farming-intensive plateau above. The presence of large fields (a striking feature in the area) and numerous greenhouses was clear from satellite imagery.

EC, alkalinity and ion concentrations were comparatively higher in borehole samples. This may have been due to longer residence times and increased water–rock interaction. Boreholes in the vicinity of the three springs (K46–47) have higher temperatures ($>30\text{ }^{\circ}\text{C}$; Table S1). They have a similar chemical signature to the cold springs (Na-HCO₃ water type; Figure 5) and comparatively high NO₃[−] concentrations (Table S2)—again likely linked to farming—but with values below the WHO drinking water recommendation of 50 mg/L [63]. However, fluoride (F[−]) concentrations largely exceeded WHO guideline of 1.5 mg/L for safe drinking water (9 to 17 times this value; Table S2 & Figure 6c). Two other boreholes were sampled twice each (in June–July 2016 and January 2017). These boreholes are located on the shore of Lake Naivasha and Crater Lake (K23 and K30 respectively; Figure 3). They have similar chemical signature samples to K46 and K47 (Na-HCO₃ water type; Figure 5), but ion concentrations were higher (Table S2 and Figure 6c). Only K30 had nitrate concentrations above detection limit but they were negligible ($<1\text{ mg/L}$). Some variability between the two sampling rounds was observed for some ions (e.g., Br[−], K[−] and Li⁺ for K23; Table S2).

4.1.3. Surface Water

Rivers displayed a wider range of EC, alkalinity values (Table 2) and ion concentrations (Table 3; Figure 6e) than groundwater samples. This variability is explained by spatial and temporal divergence. The rivers are dominantly of Na-HCO₃ water type. The only exceptions are K39 (Ca-SO₄), where water originates from a nearby dam on the Turasha River and K50 (Mixed-HCO₃), a stream that eventually flows into the Menengai Caldera (Figure 3). Ion concentrations for these two samples were in a similar range to the other river samples except for the bicarbonate concentrations of K50 (at least 2–3 times higher; Table S2 and Figure 6e). Most rivers that were sampled twice (once during the wet season—June 2016, once during the dry season—January 2017) had higher EC and ion concentrations during the dry season (Table S1). As the rivers had little to no flow during the dry season, they are subject to greater evaporation impact during this time.

The physico-chemical parameters of the lakes are very different from the rivers that feed them, except the freshwater Lake Naivasha, whose low EC values, pH, slightly alkaline (Table 2), and ionic characteristics are similar to associated rivers. Lake Naivasha is of Mixed-HCO₃ water type (Figure 5), with sodium and calcium as dominant ionic species. Samples from different depths showed no variation in ionic concentration (Table S2 and Figure 6d). The other lakes are more saline (L. Oloiden, Crater Lake, L. Nakuru and L. Elementaita in increasing order of salinity) and have alkaline pH (9.2–10) (Table 2). Lake Oloiden, Crater Lake and Lake Nakuru are all of Na-alkalinity water type (mixture of HCO₃[−] and CO₃[−]; Table S2). Lake Elementaita varies between Na-alkalinity and Na-Mixed as a result of alkalinity, chloride and fluoride in similar proportion. Most physico-chemical parameters in the lakes show limited temporal variability (narrow ranges; Table 3), although EC and ionic concentrations are higher during the dry season. Lake Nakuru was sampled a third time in June 2017 at the end of the wet season, one would have expected the EC and ion concentrations to go down, but instead an

increase was observed. Satellite imagery did not show a dramatic change of the lake area between June/July 2016 and January 2017. Between January and June 2017, the lake boundary—and presumably volume, although bathymetric data would be required for full assessment—shrank especially near the sampling areas (estimated 30 m at K25 and 90 m at K27; Figure 3). This decrease of lake area could explain the trend in increasing ionic composition observed at these sampling locations.

4.2. Stable Isotopes $\delta^{18}\text{O}$ & $\delta^2\text{H}$

Isotopic results are shown in Table S2 and Figure 7. These plots include global average [64], Kenyan Global Network of Isotopes in Precipitation (GNIP) [65], and Kenyan Rift [8] reference mean water lines. In addition, we developed our own Lake Evaporation Line (LEL) based off of calculated regression of lake $\delta^{18}\text{O}$ and $\delta^2\text{H}$ results across our three field trips. The GNIP line was calculated using results from the only two International Atomic Energy Agency (IAEA) stations available in Kenya—Kericho (c. 100 km W of Nakuru, elevation 2130 m asl, includes 24 measurements from 1967 to 1971) and Muguga (c. 125 km NE Nakuru in western suburbs of Nairobi, elevation 2070 m asl, includes 14 measurements from 1967 to 1968) [65].

The isotopic signature of rainwater samples collected on two occasions (July 2016 and June 2017) were within the same range and cluster around the GNIP meteoric water line (1.2 to 2.4‰ for $\delta^{18}\text{O}$ and 21 to 34 for $\delta^2\text{H}$; Figure 7a,c). We are therefore confident that these are good indicators of meteoric isotopic baseline values.

River samples collected in June/July 2016 during the rainy season also plot along the GNIP meteoric water line reflecting the input of rainwater. A number of perennial river sampling sites from the first trip were not sampled in January 2017 because the rivers had dried out. For those that could be sampled (not necessarily flowing rivers), a shift was observed towards enriched isotopic ratios. Sample K41 plotted close to the global meteoric water line (GMWL), but K40, K19 and K26 (which plotted very close to our LEL line) were further away, showing signs of evaporation (Figure 7b), which would explain the higher EC and concentrations observed for the samples taken in January 2017. K26, sampled a third time in June 2017 during the wet season (Figure 7c), was less enriched than in January 2017, as expected. However, it seems to have undergone some evaporation when compared to the sample taken at the same period the previous year. Rainfall data available at Nakuru meteorological station (WMO station number 637,140; data available from [66]) indicated that the wet season in 2017 was much drier than in 2016, and showed relatively little rainfall in the month preceding sampling in June 2017 (daily rain <10 mm, cumulative rainfall ~70 mm). K50 did not seem to be affected by evaporation (on the GNIP water line, Figure 7c). The difference of behaviour can be explained by the sampling location: K50 was taken in a flowing stream whereas K26 was taken in the pool at the base of Makalia Falls which had a lower flow than in 2016.

Groundwater data from borehole K30 (Figure 7a,b) and the cold springs (K50 and K61; Figure 7c) clustered along the GMWL and GNIP water lines, indicating recharge from meteoric water. Cold spring K53 and borehole K23 plotted along the lake evaporation line. K53 seems to have some input from some surface water affected by evaporation. K23 has an isotopic signature close to Lake Naivasha that would suggest groundwater mixes with lake water. However, K23 has ion concentrations about ten times greater than those from the lake. These concentrations and isotope signatures are possibly due to recharge to the aquifer by irrigation waters used in the flower farms located on the shore of Lake Naivasha.

All the lake samples were far from the GMWL and aligned well along a line defined as the Lake Evaporation Line (Figure 7). Between June/July 2016 and January 2017, all the isotope signatures shifted towards enriched isotope ratios (total average from +0.6 to +1.2‰ for $\delta^{18}\text{O}$ and +6 to +10 for $\delta^2\text{H}$), due to less inflow of isotopic-depleted waters, lower dry-season meteoric recharge, and increased evaporation. Like the rivers, increasing evaporation also explained increasing ion concentrations between the two periods. The isotopic signature of Lake Nakuru in June 2017 was further shifted towards positive values, probably a result of lake shrinking.

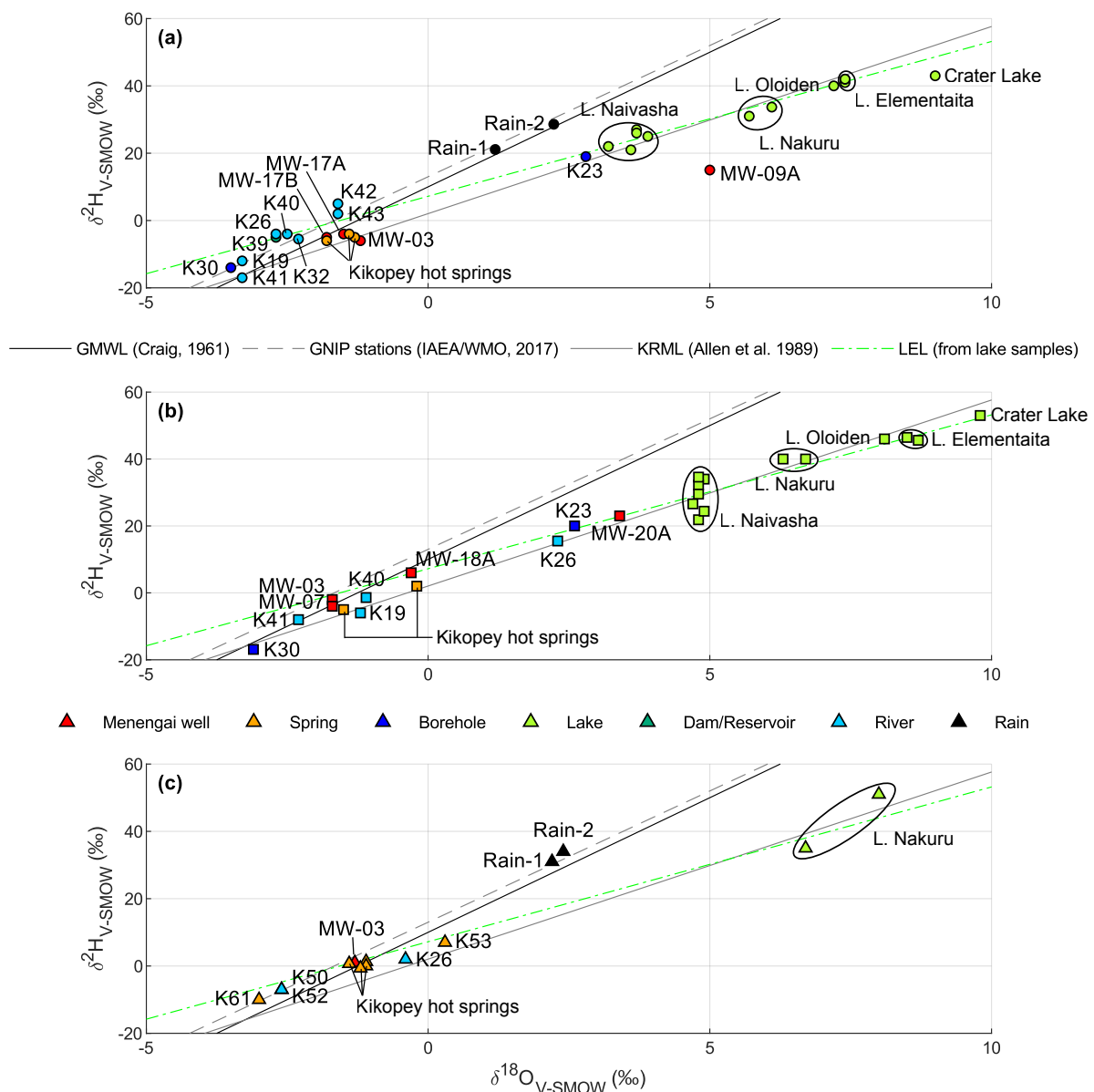


Figure 7. $\delta^{18}\text{O}$ and $\delta^2\text{H}$ data plots from the study area. (a) Sampling from June/July 2016; (b) sampling from January 2017; (c) sampling from June 2017. GMWL: Global Meteoric Water Line [64]. GNIP: Global Network of Isotopes in Precipitation data from Kericho and Muguga stations [65]. KRML: Kenya Rift Meteoric Line [8]. LEL: Lake Evaporation Line fitted by least square regression to all lake data collected by the authors.

Elementaita hot springs had similar isotope signatures (-1.8 to -0.2‰ for $\delta^{18}\text{O}$ and -6 to $+2$ for $\delta^2\text{H}$) and mostly clustered near the GMWL, except samples from January 2017. Their origin is essentially meteoric and a light shift towards higher $\delta^{18}\text{O}$ may indicate increased rock–water interactions. The samples from January 2017 were not exactly on the lake evaporation line and they were aligned on a line passing by Lake Elementaita. Their isotopic signature was probably affected by mixing with the lake during sampling (the springs are in the form of pools in direct communication with the lake).

Most isotope signatures from Menengai wells plotted along the GMWL (-1.8 to -0.3‰ for $\delta^{18}\text{O}$ and -6 to $+6$ for $\delta^2\text{H}$) indicating that the geothermal fluid comes from meteoric water. Assuming that the GNIP line is representative of rainwater in the region, this means that some rock–water interaction occurs which shifts the signature towards higher $\delta^{18}\text{O}$ values. The isotopic signature for MW-03 was consistent between the three sampling periods (-1.7 to -1.2‰ for $\delta^{18}\text{O}$ and -6 to $+1$ for $\delta^2\text{H}$). MW-18A

and MW-20A plotted on the LEL line and may indicate a stronger influence of waters sourced from Lake Nakuru to the sections of the geothermal field tapped by these wells. MW-09A was away from the LEL, and consistent with rightwards displacement, in this instance of an enriched groundwater–Lake Nakuru water mixture, that has been demonstrated to represent an exchange of oxygen between minerals and water at temperatures in excess of 150 °C [67–69].

5. Discussion

5.1. Local Meteoric Water Line

The Kenya Rift Meteoric Line (KRML) from [8] was produced using data from 22 stations (most with two sample points). The spatial distribution of stations was unclear (only the coordinates are supplied but they are in an unknown format) and their elevation ranged from 550 m to 2760 m asl. Samples were taken over a limited period between March and April 1986, and as their regression line is more closely correlated with our own LEL or the Kenya Rift Valley Evaporation Line (KRVEL) from [70] (cited in [16,42,71,72]), we believe that this data has been greatly affected by evaporation and are not representative of the recharge isotopic signature. Indeed, rain samples collected in stations at low elevation (located on the Rift floor) tend to have positive isotope signatures and depart from the GMWL compared to rain samples collected at a higher elevation (Kenyan Highlands) which tend to align along the GMWL and GNIP line. This trend was also observed by [73] on their rain samples. At the scale of East Africa, rain samples from different stations were found to cluster along the GMWL [74]. An African Meteoric Water (AMW) line was derived from non-coastal East and Central African GNIP stations by [75] and is close to the GMWL.

No consensus has been reached on the best representative LMWL, as illustrated in the literature. For Menengai studies, [17,71] used the KRML from [8] as the LMWL to interpret their results whereas [16,42] only cited it for reference in the text and on the figures. The interpretation of isotopic results was very succinct in [16] and only mentioned the KRVEL [70]. Similarly, [42] based their interpretation on the KRVEL [70] and used the Continental African Rain Line (CARL) from [70] as their LMWL (quite similar to the GMWL and the AMW). In the broader context of the Kenyan Rift Valley, some studies only used the GMWL [73,76,77] or the CARL [72,78] as a proxy for the LMWL. [79] used a LMWL similar to the GMWL and our GNIP line (same slope, intercept at +15‰). Only one study was found that used the KRML ([80], for the Olkaria geothermal field).

5.2. Comparison with Previous Studies

The seven separate Menengai production test wells of this study are of sodium–alkaline type, which is consistent with previous investigations across the caldera (references in Table 1). Ion concentrations from MW-03 were consistent with data available in the literature from the period November 2012 to June 2013 [49,50]. Ion concentrations from MW-18A were similar to literature data from the same period [56].

Isotope data available in the literature are limited to three geothermal wells, different from those sampled (MW-01, MW-04 and MW-05). MW-01 and MW-04 have a similar signature to MW-18A, plotting close to the LEL, possibly due to input from Lake Nakuru, estimated at 20% Lake Nakuru and 80% groundwater based on the present lake isotope values [42]. MW-05 is slightly off the LEL, similar to MW-09A, likely due to rock–water interaction and/or boiling [42].

5.3. Seasonal Variability

The Kikopey hot springs, situated on the edge of Lake Elementaita, maintained a consistent meteoric isotopic signature during wet-season sampling (June/July 2016 and June 2017) through the 12-month duration sampling period. Dry season analyses from January 2017 demonstrated a light shift towards higher $\delta^{18}\text{O}$ which likely represents decreased meteoric influence and entrainment of a greater proportion of lake waters in their outflow.

Groundwater from cold springs and boreholes demonstrated a consistent Na-HCO₃ ionic signature, but were split into samples that show meteoric (K30, K50, K61) and evaporitic (K23 and K53) isotopic values. K23 $\delta^{18}\text{O}$ and $\delta^2\text{H}$ were likely influenced by the mixing of the waters of Lake Naivasha, and its comparatively concentrated ion chemistry (which includes elevated nitrate and ammonium) also suggests infiltration of agricultural irrigation waters. The isotopic signature of the boreholes did not appear to be significantly affected by seasonal variability (Figure 7a,b).

Due to spatial and temporal variability, river samples demonstrated highly variable ion concentrations. Rivers that were sampled across both wet and dry seasons had higher ionic values during the dry season, demonstrating a greater influence of evaporation. This was supported by isotopic data which showed a shift towards enriched isotopic values for these locations. Lake samples also demonstrated an enriched shift in isotopic signature between wet and dry seasons due to less inflow of comparatively isotopic-depleted river waters and increased impact of evaporation. Physico-chemical properties of the lakes show limited temporal variability and are largely divergent from the rivers that feed them, and samples from different depths showed little variation. Lake Nakuru demonstrated increasing ionic composition and isotopic enrichment throughout the sampling period. Under normal circumstances, one would expect these values to reflect wet–dry season cycles; however, it appeared that the boundaries of Lake Nakuru had shrunk across the 12-month period. A decrease in lake inflow and volume could provide an explanation for this observation.

6. Conclusions

In order to fully assess the sustainability and impact of production from geothermal reservoirs, a thorough understanding of the hydrogeological systems which host targets for exploitation must be achieved. This paper presents new hydrochemical and stable isotopic insights for the Menengai Caldera geothermal field and the surrounding Nakuru County.

The sodium-alkaline dominated ionic concentration of geothermal waters from seven separate Menengai production test wells was consistent with previous investigations across the caldera. Most wells displayed $\delta^{18}\text{O}$ and $\delta^2\text{H}$ isotopic signatures associated with meteoric waters. MW-18A and MW-20A were more closely associated with the evaporative signature of the Lake Evaporation Line calculated from the lake data within this study. This suggests a greater influence of Lake Nakuru-type waters in the section of the field that these wells intersect. MW-09A showed evidence of oxygen exchange of similar waters and indicated significant water–rock interactions at temperatures in excess of 150 °C. Similar trends have been observed in other wells of the Menengai caldera [42].

The study highlights the lack of consensus regarding the Local Meteoric Water Line representative of the region around the Menengai Caldera, which is problematic for the interpretation of the isotope data and may lead to erroneous interpretation. Considering the structure of the EARS, groundwater at depth comes from recharge in the Highlands. Furthermore, most rivers in the EARS originate from the Highlands. From this perspective, the KRWL from [8] is not adequate as hinted by [76]. Available data for Kenya is limited to two stations that stopped operating almost 50 years ago and a few scattered data in the literature from one-off sampling. We advocate for the implementation of a meteorological station in the region to be sampled for isotopes.

To ensure the sustainability of the geothermal resource, understanding the hydrochemical and isotopic variability observed in the geothermal wells is critical. Geothermal wells at Menengai are regularly sampled and analysed for ion chemistry. Analysis for isotope composition does not appear to be systematic based on the existing literature. It would also be valuable to regularly sample Lake Nakuru since it is considered as a recharge source of the Menengai geothermal field. A good understanding of the variability of the isotope signature of Lake Nakuru would help refine the contribution of the lake as well as assess the sustainability of the geothermal exploitation with respect to Lake Nakuru.

The efforts detailed above represent an initial hydrochemical characterisation of surface, ground and geothermal waters in order to better understand the flow and mixing behaviour of the hydrological

system surrounding the Menengai Caldera. When combined with existing and future studies of noble gas, silica and sulphur isotopes, this data will prove to be a powerful tool in determining the sustainability and impact of soon-to-be completed, and long-term envisaged, geothermal power production operations in the Menengai Caldera.

Supplementary Materials: The following are available online at <http://www.mdpi.com/1996-1073/12/16/3131/s1>, an Excel File containing Table S1: Field data and Table S2: Lab results.

Author Contributions: Conceptualization, N.M.B., A.B. and P.L.Y.; methodology, N.M.B. and A.B.; formal analysis, N.M. (Nelly Montcoudiol), N.M.B. and A.B.; data curation, N.M. (Nelly Montcoudiol); writing—original draft preparation, N.M. (Nelly Montcoudiol) and N.M.B.; resources, T.M.; writing—review and editing, T.M., D.G., N.M. (Nicholas Mariita) and A.B.; supervision, N.M.B., N.M. (Nelly Montcoudiol), D.G., N.M. (Nicholas Mariita), T.M. and A.B.; project administration, N.M.B.; funding acquisition, N.M.B., A.B. and P.L.Y.

Funding: This research was funded by EPSRC (Engineering and Physical Sciences Research Council), grant numbers EP/P510968/1 and EP/P028829/1; and SFC (Scottish Funding Council), grant number SFC/AN/15/2016. Initial fieldwork and analysis was supported by the Geological Society of London and the Glasgow Natural History Society. N.M.B. is funded by a University of Glasgow LKAS Research Fellowship; A.B. is funded by ICSF at SUERC (NERC Facility contract F14/G6/11/01).

Acknowledgments: The authors would like to acknowledge the late Paul L. Younger (P.L.Y.) for inspiring and helping to secure funding for the work; Anne McGarity and Alison McDonald for analyses; GDC for access to the Menengai Caldera; Freena Garcia for help with GIS mapping of faults and lake levels; and the Kenya 2016 UoG students for sampling and sample preparation assistance.

Conflicts of Interest: The authors declare no conflict of interest and the funders had no role in the design of the study; in the collection, analyses, or interpretation of data; in the writing of the manuscript, or in the decision to publish the results.

References

- Alexander, K.B.; Ussher, G. Geothermal resource assessment for Mt Longonot, Central Rift Valley, Kenya. In Proceedings of the GRC Annual Meeting, San Diego, CA, USA, 23–26 October 2011; pp. 1147–1154.
- Teklemariam, M. Geothermal outlook in East Africa and contribution of UNU-GTP in capacity building. In Proceedings of the 40th Anniversary Workshop of UNU-GTP, Reykjavik, Iceland, 26 April 2018.
- Omenda, P.; Mangi, P. Country update report for Kenya—2016. In Proceedings of the 6th African Rift Geothermal Conference, Addis Ababa, Ethiopia, 31 October–6 November 2016.
- IEA. *Electricity Generation by Fuel*; International Energy Agency: Paris, France, 2019.
- Richter, A. KenGen Announces 86.6 MW of Olkaria V Unit 1 Geothermal Plant to Be Online. Available online: <http://www.thinkgeoenergy.com/kengen-announces-86-6-mw-of-olkaria-v-unit-1-geothermal-plant-to-be-online/> (accessed on 31 July 2019).
- Omenda, P.; Simiyu, S. Country update report for Kenya 2010–2014. In Proceedings of the World Geothermal Congress 2015, Melbourne, Australia, 19–24 April 2015.
- Baker, B.H. Tectonics and volcanism of the southern Kenya Rift Valley and its influence on rift sedimentation. *Geol. Soc. Lond. Spec. Publ.* **1986**, *25*, 45–57. [[CrossRef](#)]
- Allen, D.J.; Darling, W.G.; Burgess, W.G. *Geothermics and Hydrology of the Southern Part of the Kenya Rift Valley with Emphasis on the Magadi-Nakuru Area*; SD/89/1; British Geological Survey: Nottingham, UK, 1989.
- Burke, K.; Dewey, J.F. Plume-Generated Triple Junctions: Key Indicators in Applying Plate Tectonics to Old Rocks. *J. Geol.* **1973**, *81*, 406–433. [[CrossRef](#)]
- Wameyo, P.M. *Magnetotelluric and Transient Electromagnetic Methods in Geothermal Prospecting, with Examples from Menengai, Kenya*; The United Nations University: Reykjavik, Iceland, 2005; pp. 409–439.
- Omenda, P.A. Status of geothermal exploration in Kenya and future plans for its development. In Proceedings of the Short Course II on Surface Exploration for Geothermal Resources, Lake Naivasha, Kenya, 2–17 November 2008.
- Kanda, I. Geochemical exploration of geothermal prospects: A case study of Menengai, Kenya. In Proceedings of the Short Course VIII on Exploration for Geothermal Resources, Lake Naivasha, Kenya, 31 October–23 November 2013.
- Leat, P.T.; Macdonald, R.; Smith, R.L. Geochemical evolution of the Menengai Caldera Volcano, Kenya. *J. Geophys. Res. Space Phys.* **1984**, *89*, 8571–8592. [[CrossRef](#)]

14. Macdonald, R.; Navarro, J.; Upton, B.; Davies, G. Strong compositional zonation in peralkaline magma: Menengai, Kenya Rift Valley. *J. Volcanol. Geotherm. Res.* **1994**, *60*, 301–325. [[CrossRef](#)]
15. Jirsa, F.; Gruber, M.; Stojanovic, A.; Omondi, S.O.; Mader, D.; Körner, W.; Schagerl, M. Major and trace element geochemistry of Lake Bogoria and Lake Nakuru, Kenya, during extreme draught. *Geochemie* **2013**, *73*, 275–282. [[CrossRef](#)] [[PubMed](#)]
16. Kanda, I.; Suwai, J. Hydrogeochemistry of shallow and deep water aquifers of Menengai geothermal area, Kenya Rift Valley. In Proceedings of the GRC Annual Meeting, Las Vegas, NV, USA, 29 September–2 October 2013; pp. 403–409.
17. Igunza, G.M.; Kanda, I. Geochemical evaluation of groundwater flow processes and mixing in Menengai geothermal field, Kenya. In Proceedings of the GRC Annual Meeting, Salt Lake City, UT, USA, 1–4 October 2017.
18. Raini, J.A. Impact of land use changes on water resources and biodiversity of Lake Nakuru catchment basin, Kenya. *Afr. J. Ecol.* **2009**, *47*, 39–45. [[CrossRef](#)]
19. WRI. Kenya GIS Data. Available online: <http://www.wri.org/resources/data-sets/kenya-gis-data> (accessed on 10 January 2017).
20. Munyiri, S.K. *Structural Mapping of Olkaria Domes Geothermal Field Using Geochemical Soil Gas Surveys, Remote Sensing and GIS*; School of Engineering and Natural Sciences, University of Iceland: Reykjavík, Iceland, 2016.
21. Kaishan. *Milestone Achieved by Kaishan in Its Exploration of Overseas Geothermal Power Generation Markets*; Zhejiang Kaishan Compressor Co., Ltd.: Hangzhou, China, 2017.
22. Gaciri, S.; Davies, T. The occurrence and geochemistry of fluoride in some natural waters of Kenya. *J. Hydrol.* **1993**, *143*, 395–412. [[CrossRef](#)]
23. Darling, W.; Griesshaber, E.; Andrews, J.; Armannsson, H.; O’Nions, R. The origin of hydrothermal and other gases in the Kenya Rift Valley. *Geochim. Cosmochim. Acta* **1995**, *59*, 2501–2512. [[CrossRef](#)]
24. Furman, T. Geochemistry of East African Rift basalts: An overview. *J. Afr. Earth Sci.* **2007**, *48*, 147–160. [[CrossRef](#)]
25. Marty, B.; Gunnlaugsson, E.; Jambon, A.; Oskarsson, N.; Ozima, M.; Pineau, F.; Torssander, P. Gas geochemistry of geothermal fluids, the Hengill area, southwest rift zone of Iceland. *Chem. Geol.* **1991**, *91*, 207–225. [[CrossRef](#)]
26. Lollar, B.S.; Ballentine, C.; Onions, R. The fate of mantle-derived carbon in a continental sedimentary basin: Integration of relationships and stable isotope signatures. *Geochim. Cosmochim. Acta* **1997**, *61*, 2295–2307. [[CrossRef](#)]
27. Allen, D.J.; Darling, W.G. *Geothermics and hydrogeology of the Kenya Rift Valley between Lake Baringo and Lake Turkana*; SD/92/001; British Geological Survey: Nottingham, UK, 1992; p. 133.
28. Rogers, N. Two mantle plumes beneath the East African rift system: Sr, Nd and Pb isotope evidence from Kenya Rift basalts. *Earth Planet. Sci. Lett.* **2000**, *176*, 387–400. [[CrossRef](#)]
29. Baker, B.H.; Wohlenberg, J. Structure and Evolution of the Kenya Rift Valley. *Nature* **1971**, *229*, 538–542. [[CrossRef](#)] [[PubMed](#)]
30. Girdler, R.W.; Sowerbutts, W.T.C. Some recent geophysical studies of the Rift System in East Africa. *J. Geomagn. Geoelectr.* **1970**, *22*, 153–163. [[CrossRef](#)]
31. Khan, M.A.; Mansfield, J. Gravity Measurements in the Gregory Rift. *Nat. Phys. Sci.* **1971**, *229*, 72–75. [[CrossRef](#)]
32. Searle, R.C. Evidence from Gravity Anomalies for Thinning of the Lithosphere beneath the Rift Valley in Kenya. *Geophys. J. Int.* **1970**, *21*, 13–31. [[CrossRef](#)]
33. Wambugu, J.M. Chemistry in exploration of a geothermal field. In Proceedings of the Short Course IV on Exploration for Geothermal Resources, Lake Naivasha, Kenya, 1–22 November 2009.
34. Lagat, J. Geothermal surface exploration approach: Case study of Menengai geothermal field, Kenya. In Proceedings of the Kenya Geothermal Conference, Nairobi, Kenya, 21–23 November 2011.
35. Shako, L.; Wamalwa, A. GIS applications in heat source mapping in Menengai geothermal field. In Proceedings of the 5th African Rift Geothermal Conference, Arusha, Tanzania, 29–31 October 2014.
36. Simiyu, S.M. Application of micro-seismic methods to geothermal exploration: Examples from the Kenya Rift. In Proceedings of the Short Course VIII on Exploration for Geothermal Resources, Lake Naivasha, Kenya, 31 October–23 November 2013.

37. Malimo, S.J. Use of radon and carbon dioxide in geochemical exploration of Menengai and Silali geothermal prospects, Kenya. In Proceedings of the 4th African Rift Geothermal Conference, Nairobi, Kenya, 21–23 November 2012.
38. Mibei, G. Geothermal exploration of the Menengai geothermal field. In Proceedings of the Short Course X on Exploration for Geothermal Resources, Lake Naivasha, Kenya, 9–30 November 2015.
39. Omenda, P.A. Geothermal development in Kenya: A country update—2012. In Proceedings of the 4th African Rift Geothermal Conference, Nairobi, Kenya, 21–23 November 2012; pp. 89–93.
40. Suwai, J.J. *Preliminary Reservoir Analysis of Menengai Geothermal Field Exploration Wells*; The United Nations University: Reykjavík, Iceland, 2011; pp. 799–826.
41. Mangi, P.M. Geothermal development in Kenya—Country updates. In Proceedings of the 7th African Rift Geothermal Conference, Kigali, Rwanda, 29 October–4 November 2018.
42. Sekento, L.R. *Geochemical and Isotopic Study of the Menengai Geothermal Field, Kenya*; The United Nations University: Reykjavík, Iceland, 2012; pp. 769–792.
43. Gichira, J. Joint 1D inversion of MT and TEM data from Menengai geothermal field, Kenya. In Proceedings of the 5th African Rift Geothermal Conference, Arusha, Tanzania, 29–31 October 2014.
44. Kanda, I.; Fujimitsu, Y.; Nishijima, J. Geological structures controlling the placement and geometry of heat sources within the Menengai geothermal field, Kenya as evidenced by gravity study. *Geothermics* **2019**, *79*, 67–81. [[CrossRef](#)]
45. Montegrossi, G.; Pasqua, C.; Battistelli, A.; Mwawongo, G.; Ofwona, C. 3D natural state model of the Menengai geothermal system, Kenya. In Proceedings of the World Geothermal Congress 2015, Melbourne, Australia, 19–24 April 2015.
46. Standard Reporter. *Nakuru Power Project Now Set for September*; Available online: <https://www.standardmedia.co.ke/business/article/2001289112/nakuru-power-project-to-start-in-september> (accessed on 23 July 2018).
47. Takouleu, J.M. Kenya: Zhejiang Kaishan to Build Menengai III Geothermal Power Plant. *Afrik21*, 15 April 2019.
48. Kipng'ok, J. *Fluid Chemistry, Feed Zones and Boiling in the First Geothermal Exploration Well at Menengai, Kenya*; The United Nations University: Reykjavík, Iceland, 2011; pp. 281–302.
49. Malimo, S.J. Fluid chemistry of Menengai geothermal wells, Kenya. In Proceedings of the GRC Annual Meeting, Las Vegas, NV, USA, 29 September–2 October 2013; pp. 425–429.
50. Auko, L.O. *Evaluation of Fluid—Mineral Interaction in the Menengai Geothermal System, Central Rift, Kenya*; The United Nations University: Reykjavík, Iceland, 2014; pp. 39–64.
51. Kipng'ok, J.; Ochieng, L.; Kanda, I.; Suwai, J. Characterization of the Menengai high temperature geothermal reservoir using gas chemistry. In Proceedings of the GRC Annual Meeting, Portland, OR, USA, 26–28 May 2014; pp. 445–451.
52. Malimo, S.J. Geochemical monitoring practices. In Proceedings of the Short Course IX on Exploration for Geothermal Resources, Lake Naivasha, Kenya, 2–23 November 2014.
53. Auko, L.O.; Kipngok, J.K.; Mibei, G.K.; Kanda, I.K. Chemical Composition of Fumarolic Gases at the Menengai Geothermal Field-Central Rift Kenya: Variations monitored over a period of sampling from the year 2009 to June 2013. In Proceedings of the World Geothermal Congress 2015, Melbourne, Australia, 19–24 April 2015.
54. Mundui, J.K.K. *Mineral Scaling Potential Of Geothermal Fluids in Well MW 01A in Menengai, Kenya*; The United Nations University: Reykjavík, Iceland, 2015; pp. 533–548.
55. Kipngok, J.; Suwai, J.; Auko, L.; Malimo, S.; Mulusa, G.; Chepkemoi, S.; Marini, L. Assessment of carbon dioxide (CO₂) partial pressures in the Menengai geothermal area, Kenya. In Proceedings of the 7th African Rift Geothermal Conference, Kigali, Rwanda, 29 October–4 November 2018.
56. Njue, L.; Kipngok, J. Menengai Geothermal Field—Eastern Upflow. In Proceedings of the 7th African Rift Geothermal Conference, Kigali, Rwanda, 29 October–4 November 2018.
57. USGS. Earth Explorer. Available online: <https://earthexplorer.usgs.gov/> (accessed on 27 June 2019).
58. Burnside, N.; Banks, D.; Boyce, A.; Athresh, A. Hydrochemistry and stable isotopes as tools for understanding the sustainability of minewater geothermal energy production from a 'standing column' heat pump system: Markham Colliery, Bolsover, Derbyshire, UK. *Int. J. Coal Geol.* **2016**, *165*, 223–230. [[CrossRef](#)]
59. Misstear, B.D.R.; Banks, D.; Clark, L. *Water Wells and Boreholes*, 2nd ed.; John Wiley & Sons Ltd.: Chichester, UK, 2017; p. 536.

60. Younger, P. *Groundwater in the Environment*; Blackwell Publishing: Hoboken, NJ, USA, 2007.
61. Gonfiantini, R.I.A.E.A. advisory group meeting on stable isotope reference samples for geochemical and hydrological investigations: Vienna, Austria, September 19–21, 1983. *Chem. Geol.* **1984**, *46*, 85. [[CrossRef](#)]
62. Andhika, M.; Castañeda, M.H.; Regenspurg, S. Characterization of Silica Precipitation at Geothermal Conditions. In Proceedings of the World Geothermal Congress 2015, Melbourne, Australia, 19–24 April 2015.
63. WHO. *Global Health Observatory Indicator Views*; World Health Organization: Geneva, Switzerland, 2018.
64. Craig, H. Isotopic Variations in Meteoric Waters. *Science* **1961**, *133*, 1702–1703. [[CrossRef](#)]
65. IAEA/WMO. *Global Network of Isotopes in Precipitation*; IAEA/WMO: Geneva, Switzerland, 2019.
66. NCDC. *NCDC Climatic Data Online*; National Climatic Data Centre: Asheville, NC, USA, 2019.
67. Craig, H. The isotopic geochemistry of water and carbon in geothermal areas. In *Nuclear Geology on Geothermal Areas*; Consiglio Nazionale Delle Ricerche (CNR): Spoleto, Italy, 1963; pp. 17–53.
68. D’Amore, F.; Panichi, C. Geochemistry in geothermal exploration. *Int. J. Energy Res.* **1985**, *9*, 277–298. [[CrossRef](#)]
69. Nicholson, K. *Geothermal Fluids: Chemistry and Exploration Techniques*; Springer: Berlin/Heidelberg, Germany, 1993. [[CrossRef](#)]
70. Ármannsson, H. *Geochemical Studies on Three Geothermal Areas in West and Southwest, Uganda—Final Report*; UGA/92/003; UNDES, GSMD: Entebbe, Uganda; New York, NY, USA, 1994.
71. Mutonga, M.W. Stable isotopic composition of geothermal fields in Kenya: The relationship between geothermal fields and Kenya Rift lakes waters. In Proceedings of the World Geothermal Congress 2015, Melbourne, Australia, 19–24 April 2015.
72. Nkapiiani, M.N.; Kamunya, K.M. Application of Stable Isotope Geochemistry to Tracing Recharge and Flow Systems of Fluids in Olkaria Geothermal Field, Kenya. In Proceedings of the Stanford Geothermal Workshop, Stanford, CA, USA, 26–28 January 2015.
73. Ojiambo, B.S.; Poreda, R.J.; Lyons, W.B. Ground Water/Surface Water Interactions in Lake Naivasha, Kenya, Using $\delta^{18}\text{O}$, δD , and $3\text{H}/3\text{He}$ Age-Dating. *Ground Water* **2001**, *39*, 526–533. [[CrossRef](#)] [[PubMed](#)]
74. Rozanski, K.; Araguas-Araguas, L.; Gonfiantini, R. Isotope patterns of precipitation in the East African region. In *The Limnology, Climatology and Paleoclimatology of the East African Lakes*; Johnson, T.C., Odada, E.O., Eds.; Gordon and Breach Publishers: Amsterdam, The Netherlands, 1996; pp. 79–93.
75. Cohen, A.S.; Talbot, M.R.; Awramik, S.M.; Dettman, D.L.; Abell, P. Lake level and paleoenvironmental history of Lake Tanganyika, Africa, as inferred from late Holocene and modern stromatolites. *GSA Bull.* **1997**, *109*, 444–460. [[CrossRef](#)]
76. Ojiambo, B.S.; Lyons, W.B. Stable Isotope Composition of Olkaria Geothermal Fluids, Kenya. *Geotherm. Resour. Counc. Trans.* **1993**, *17*, 149–154.
77. Olaka, L.A.; Wilke, F.D.; Olago, D.O.; Odada, E.O.; Mulch, A.; Musolff, A. Groundwater fluoride enrichment in an active rift setting: Central Kenya Rift case study. *Sci. Total Environ.* **2016**, *545*, 641–653. [[CrossRef](#)] [[PubMed](#)]
78. Nkapiiani, M.N. *Application of Stable Isotope Geochemistry to Tracing Recharge and Flow Systems of Fluids in the Olkaria Geothermal Field, Kenya*; United Nations University: Reykjavik, Iceland, 2014.
79. Cioni, R.; Fanelli, G.; Guidi, M.; Kinyariro, J.; Marini, L. Lake Bogoria hot springs (Kenya): Geochemical features and geothermal implications. *J. Volcanol. Geotherm. Res.* **1992**, *50*, 231–246. [[CrossRef](#)]
80. Karingithi, C.W. *Geochemical Characteristics of the Greater Olkaria Geothermal Field, Kenya*; The United Nations University: Reykjavik, Iceland, 2000; pp. 165–188.

